THE JOURNAL OF PHYSICAL CHEMISTRY C

Article

pubs.acs.org/JPCC

Superparamagnetic FeCo and FeNi Nanocomposites Dispersed in Submicrometer-Sized C Spheres

E. M. M. Ibrahim,*[,†,‡] Silke Hampel,[†] A. U. B. Wolter,[†] M. Kath,[§] A. A. El-Gendy,[†,§] R. Klingeler,[§] Christine Täschner,[†] Vyacheslav O. Khavrus,[†] Thomas Gemming,[†] Albrecht Leonhardt,[†] and Bernd Büchner[†]

[†]Leibniz Institute of Solid State and Material Research Dresden, P.O. Box 270016, D-01171 Dresden, Germany

[‡]Department of Physics, Faculty of Science, Sohag University, Sohag-82524, Egypt

[§]Kirchhoff Institute for Physics, University of Heidelberg, INF 227, D-69221 Heidelberg, Germany

ABSTRACT: Magnetic spheres with average diameter 100 nm, consisting of FeCo and FeNi nanomagnets (with average diameters 5.9 ± 1 and 4.6 ± 0.3 nm, respectively) dispersed in spherical carbon colloid have been synthesized using the radio frequency plasma-enhanced chemical vapor deposition technique. The nanoparticles are tightly embedded in the C matrix and well protected from oxidation. Superparamagnetic features such as typical Langevin-like magnetization curves are observed for the nanocomposites. A comprehensive analysis of the presence of dipolar interactions has been carried out within the framework of the mean-field model. The size of the nanoparticles constituting the carbon-spheres is near to the optimal value where Néel losses are maximal and considerable Neel-type specific absorption rates are observed. The material may hence provide a new material-based approach to realize biocompatibly protected superparamagnetic beads for application in biological environments, in particular, for magnetic hyperthermia.

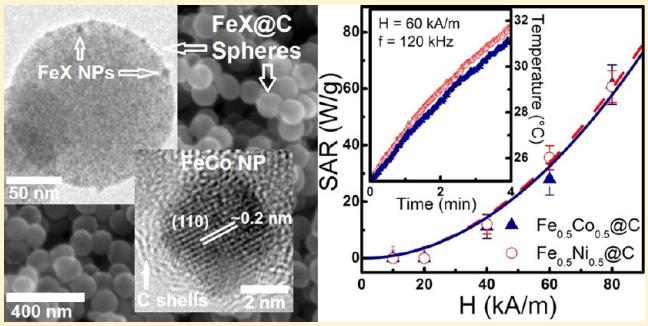

INTRODUCTION

Recently, fabrication of superparamagnetic colloidal composites has a renewed interest worldwide, driven by the excitement of understanding new science and the growth in their applications in different fields such as catalysis and bioscience.[1,2] The fascinating properties revealed by the magnetic nanocomposites are emerged due to the combination of the magnetic nanoparticles and the colloidal matrices: the nanocomposites acquire magnetic functionality such as monitoring, heating, and guiding from the magnetic nanoparticles, while the matrices improve the chemical stability, chemical functionality, and biocompatibility.[3]

The potential applicability of a magnetic nanocomposite varies widely depending on its magnetic properties. Actually, various factors can tune the magnetism in the composite. A main issue are the individual properties of the magnetic nanoparticles including chemical composition, size, and shape. For instance, the nanoparticles of FeCo and FeNi alloys that have been addressed in this work are of particular interest due to their high saturation magnetization, large permeability, and hence, high magnetophoretic mobility,[4,5] which may be applied as magnetic carriers for in vitro separation and therapeutic in vivo technology.[6,7]

The second factor is the nanoparticles distribution in the colloidal matrix (i.e., whether the nanoparticles are rather isolated or considerably magnetically interacting). For isolated noninteracting superparamagnetic nanoparticles, the magnetic behavior can be described on the basis of Néel arguments, namely, the magnetization reversal through a thermally activated process over the anisotropy barrier, even in the absence of an externally applied field.[8] The noninteracting behavior can be realized for sufficiently diluted nanocomposites with low volume fraction and highly dispersed nanoparticles in the whole colloidal matrix. In such systems where the interparticle interactions are negligible, the crossover to the blocked state with decreasing temperature depends only on the physical properties of individual particles.[9,10] However, when the interparticle interactions become significant, the process becomes more complicated where the magnetic response is not only governed by its own intrinsic anisotropy energy but also by coupling with its neighbors.[11] It is worth noting that, for diluted composites, only the synthesizing method can guarantee a fixed minimum distance between the magnetic nanoparticles and, hence, the absence of significant magnetic interaction between them.[12] The synthesizing method guarantees also the biostability of the magnetic nanomaterial because noncoated magnetic materials tend to chemically interact with biological environments, thereby forming, for

Received: May 2, 2012
Revised: September 9, 2012
Published: September 13, 2012

   dx.doi.org/10.1021/jp304236x | J. Phys. Chem. C 2012, 116, 22509−22517

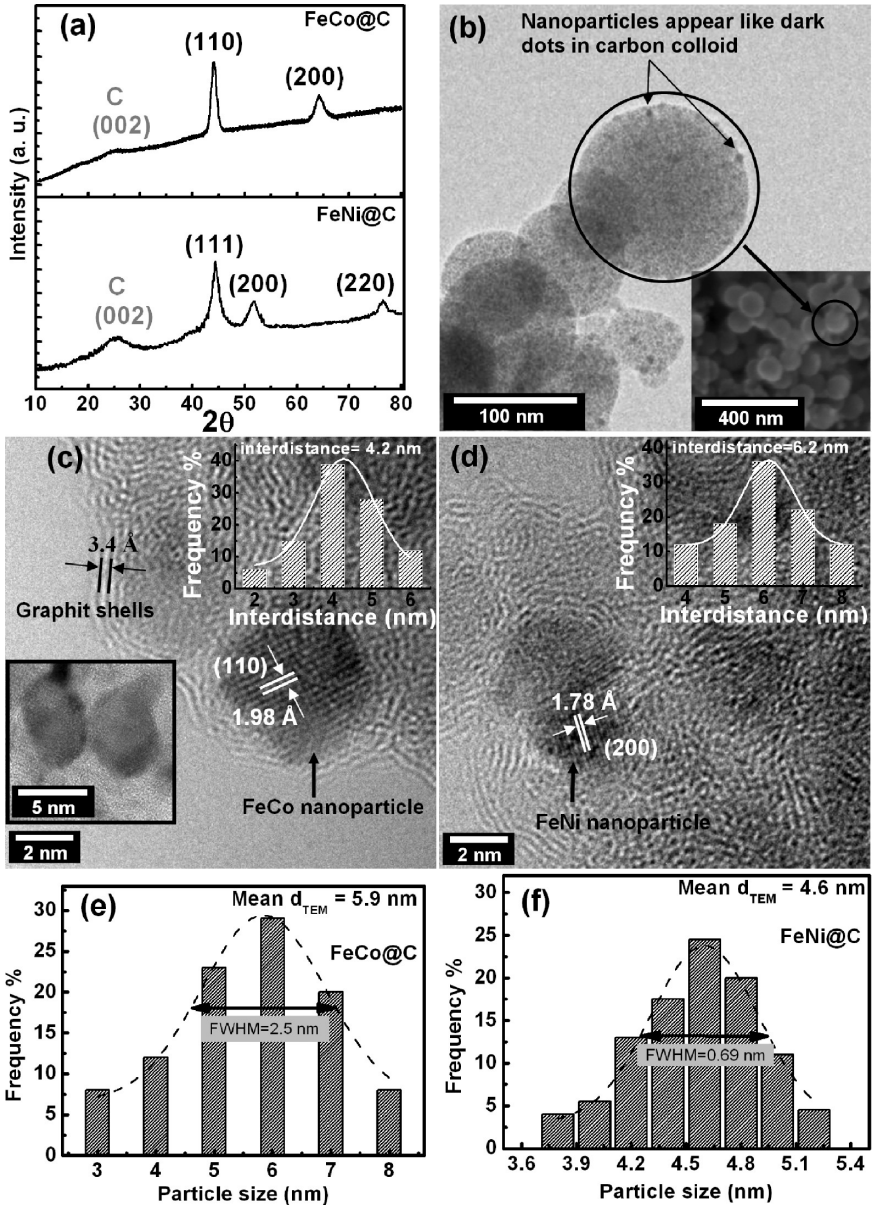

Figure 1. (a) XRD diffractograms of the synthesized nanocomposites; (b) HRTEM image of a collection of FeCo@C spheres as an example (the inset is a HRSEM image); (c, d) HRTEM images at higher magnification showing the morphology of one sphere of FeCo@C and FeNi@C, respectively (the histograms inserted as insets show the distribution of interdistance between the nanoparticles embedded in the C spheres of the corresponding nanocomposites, while the left inset of (c) is a HRTEM image showing two FeCo nanoparticles in direct contact); (e, f) Histograms represent the size distribution of the nanoparticles.

example, oxide layers at the particle surface that causes changes in the materials magnetic properties (due to the exchange coupling between the particle core and the oxide shell),[13,14] as well as potentially toxic oxidative stress to the environment. Another factor tuning the magnetism in the nanocomposite is the nanomagnet−matrix interaction where the magnitude of the dipolar interactions strongly depends on the textural characteristics of the matrices in which the nanomagnets are dispersed. For example, Rebolledo et al.[1] demonstrated that lower matrix densities led to a reduction in the magnitude of dipolar interactions.

In this work, two different C-based nanocomposites of FeCo and FeNi nanoparticles have been synthesized using a facile method based on carrying out simultaneous sublimation and activation processes for metallocenes in radio frequency (rf) plasma field followed by a thermal decomposition process. The collected materials consist of submicrometer-sized spheres. Each sphere consists of C colloid containing inside a set of randomly dispersed spherical magnetic nanoparticles (FeCo or FeNi). The syntheses method guarantees well magnetic isolation of the nanoparticles by keeping a minimal separating distance between them in the C matrix. We present a study on the morphology and magnetic properties of the synthesized nanocomposites. Furthermore, the dipolar interactions and the heating response in the AC magnetic field were determined to investigate and quantify the feasibility of using the nanocomposites as hyperthermia agents.

dx.doi.org/10.1021/jp304236x | J. Phys. Chem. C 2012, 116, 22509−22517

EXPERIMENTAL SECTION

The $Fe_{50}Co_{50}$@C and $Fe_{50}Ni_{50}$@C nanocomposites have been synthesized by means of an inductively coupled rf plasma supporting thermal decomposition of ferrocene/cobaltocene or ferrocene/nickelocene mixtures, respectively. The used device consists of a quartz tube (internal diameter 3 cm, total length 90 cm) equipped with two separate zones. The metallocenes are placed in a radio frequency rf plasma field (first zone) ignited through a circular coil using a 180 W Hüttinger rf generator type PFG 1000 RF (with power 50 W) to make sublimation and partial decomposition. For completing the decomposition process and by using an argon gas stream (flow rate of 20 sccnm), the partially decomposed precursors are transported into the second zone (which is a hot zone of 600 °C). Because of the argon flow, the obtained material deposits inside a short quartz tube placed at 5 cm outside the hot zone. It is worth noting that the precursor concentration in the gas phase during the synthesis processes was estimated to be 4.4×10^{-6} and 2.9×10^{-6} g/cm^3 for ferrocene/cobaltocene and ferrocene/nickelocene mixtures, respectively. After finishing the deposition process and to protect the synthesized nanocomposites against oxidation, a magnetic manipulator was utilized to displace the short quartz tube, on which the material deposit, to the hot zone for doing the coating process. The coating process was carried out in the hot zone at 600 °C using a gas stream consisting of 80% argon and 20% ethylene as a carbon source. Both the temperature and the argon/ethylene ratio were found to be optimal for the ethylene decomposition without growing carbon nanotubes.

Scanning electron microscopy (SEM) analysis was performed by means of a FEI- NANOSEM-200 with acceleration voltage of 15 kV. High-resolution transmission electron microscopy investigation (HRTEM) and EDX analyses were carried out using a FEI Tecnai F 30 TEM with Schottky field emission gun at 300 kV equipped with an EDAX Si (Li) energy dispersive X-ray detector. To identify the crystal structure, a Miniflex X-ray diffractometer (XRD) with Cu K_α radiation (λ = 1.5418 Å) was used at room temperature. The magnetic properties were determined with a commercial Superconducting Quantum Interference Device magnetometer (VSM-SQUID) from Quantum Design. The magnetic field dependence of the magnetization was measured at different temperatures for external magnetic field up to 3 T. The temperature dependence of the magnetization was determined in both field cooling (FC) and zero field cooling (ZFC) regimes. In the ZFC case, the samples were first cooled in zero magnetic field to 5 K and then a magnetic field of 100 Oe was applied to the samples. In such a ZFC condition, the measurements were performed upon heating up to 400 K. The FC data were obtained within the same temperature range after cooling the sample in the same field. The heating effect of AC magnetic fields was studied by means of a home-built setup consisting of a high frequency generator with water-cooled magnetic coil system at a frequency of 120 kHz and magnetic field strengths of 0−100 kA/m and a fiber-optical thermometer.[15]

RESULTS AND DISCUSSION

Sample Characterization. Figure 1a shows the XRD patterns of the FeCo@C and FeNi@C nanocomposites. The diffraction peaks are corresponding to typical bcc structure of FeCo and fcc structure of FeNi alloys phases, confirming the expected crystal structure. The small broad hump at $2\theta = 26°$ is attributed to the graphitic carbon shells. No indications of oxide or carbide phases were detected. The rather large width of the diffraction peaks indicates the small size of the nanoparticles. Assuming that the nanoparticles have spherical shape and according to Scherrer's equation, $D = 0.89\lambda/\beta \cos \theta$,[16] the crystallite size of the nanoparticles can be calculated from the full width at half-maximum β of the diffraction peak corresponding to the Bragg angle θ. Taking into account the wavelength of Cu K_α radiation λ = 1.5418 Å yields the mean diameters d_{XRD} equal to 6.4 ± 1 and 5.3 ± 1 nm for the FeCo and FeNi nanoparticles in the carbon spheres, respectively.

The inset of Figure 1b displays a scanning electron microscope (SEM) image of FeCo@C. Note that, no significant differences in the overall morphology of both FeCo@C and FeNi@C samples were observed. The images in Figure 1b imply that the material consists of individual submicrometer-sized spheres. The magnetic nanoparticles which appear as dark dots in Figure 1b are dispersed randomly in a carbon colloid which is the building block of the spheres. The morphology of the individual nanoparticles in both FeCo@C and FeNi@C is highlighted by the HRTEM images in Figure 1c,d. In general, the images confirm that the particles are well coated by carbon. To be specific, Figure 1c,d clearly implies good crystallinity of the core crystallites by the appearance of fringes of the lattice planes (marked in the figures by white short parallel lines). Noteworthy, the bcc structure of FeCo and fcc structure of FeNi crystal planes could be clearly identified with an interplanar distance of 1.98 Å (110) and 1.78 Å (200), respectively. In addition, in some places the images imply concentric carbon shells (corresponding to (002) graphitic planes) surrounding the core nanoparticles but these shells are not uniform and in most instances only poorly crystalline or in an amorphous state.

In addition, the size and size distribution of the nanoparticles can be extracted from the TEM images. The results of this analysis are displayed in Figure 1e,f. The nanoparticles size distribution in FeCo@C ranges from 3 to 8 nm, with an average value of 5.9 ± 1 nm. The respective histogram for FeNi@C implies a smaller size distribution ranging from 3.8 to 5.2 nm, while the average diameter amounts to d_{TEM} = 4.6 ± 0.3 nm. Note, that both values agree to those determined from the XRD patterns.

The HRTEM images confirm the composite nature of the deposited materials. To be more specific, in the case of FeNi@C the nanoparticles in the spheres are separated by carbon shells. We found average interdistances between the FeNi nanoparticles of 6.2 ± 1.3 nm (see the histogram in Figure 1d) and no particle−particle contact was observed. For FeCo@C, the majority of the nanoparticles are well separated (the mean interparticle distance is 4.2 ± 1 nm, as seen in the histogram depicted in Figure 1c). However, irrespective of the particle size there are a few neighboring particles being either nearly or actually in contact but forming separate grains without coalescence (see left inset of Figure 1c). The smaller interparticle distance in FeCo@C may be attributed to the higher precursor concentration in the gas phase, 4.4×10^{-6} g/cm^3, during the synthesis process in comparison to 2.9×10^{-6} g/cm^3 in the case of FeNi@C synthesis.

The core particle composition was confirmed by EDX analysis to be $Fe_{50}Co_{50}$ and $Fe_{50}Ni_{50}$. It was found that the alloy chemical composition can be controlled by varying the initial ratios of the metallocenes placed in the plasma field. For example, producing FeCo or FeNi alloys with atomic

dx.doi.org/10.1021/jp304236x | J. Phys. Chem. C 2012, 116, 22509−22517

percentage of about 50:50 was achieved with initial ratios 1:1 of the ferrocene/cobaltocene or ferrocene/nickelocene, respectively.

Magnetic Properties. *Magnetization as a Function of Temperature.* The temperature dependences of the magnetization measured in the range between 5 and 400 K in both field cooling (FC) and zero field cooling (ZFC) regimes under magnetic field of H = 100 Oe for FeCo@C and FeNi@C samples are shown in Figure 2. Two characteristic features are

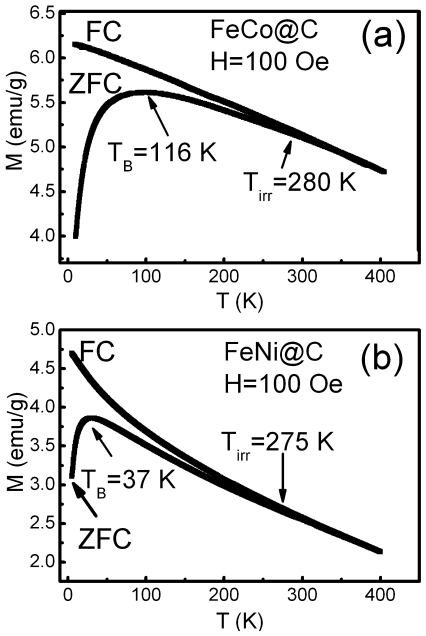

Figure 2. ZFC and FC magnetization curves measured at magnetic fields 100 Oe for the (a) FeCo@C and (b)FeNi@C nanocomposites.

expected from magnetization data of superparamagnetic systems: (1) A paramagnetic-like behavior at high temperatures and (2) a rounded maxima in the ZFC curves at a temperature T_{max}.[17] For noninteracting particles, T_{max} is directly proportional to the average blocking temperature T_B with a proportionality constant β = 1−2 that depends on the type of size distribution. Therefore, T_{max} is related to the blocking of particles with the mean particle size.[9,10] For our samples, the $M_{ZFC}(T)$ curves exhibit broad maxima for FeCo@C nanocomposite (see Figure 2a), suggesting that there is a distribution of blocking temperatures rather than a well-defined value for T_B. This implies a broad distribution of particle sizes and hence of energy barriers. In contrast, $M_{ZFC}(T)$ curves of the FeNi@C samples that exhibit a more narrow size distribution show well-defined features that allow to extract T_B well (see Figure 2b). To be specific, from the maxima of the ZFC magnetization curve we extract T_B = 116 and 37 K for FeCo@C and FeNi@C, respectively. Assuming the spherical shape of the magnetic nanoparticle, the magnetic anisotropy constant can be roughly estimated by using the relationship[18]

$$T_B = K_{eff}\langle V\rangle/25k_B \quad (1)$$

where K_{eff} is the effective magnetic anisotropy constant, $\langle V\rangle$ is the average volume, and k_B is the Boltzmann constant. By using the experimental values of T_B and d_{TEM}, magnetic anisotropy constants values of 3.8×10^5 and 2.5×10^5 J m^{3-} are estimated for FeCo@C and FeNi@C samples, respectively. These anisotropy values are higher by 2 orders of magnitude as compared to the bulk values.[19,20] Such a strong enhancement of the effective magnetic anisotropy upon downscaling bulk materials has been observed for several magnetic materials, for example, in ultrafine $CoFe_2O_4$[21] or NiRu@C[22] and it is often ascribed to surface anisotropy. In the example of the FeCo alloys, Peng et al. report nonmonotonous size effects on K_{eff} as changing the diameter of $Fe_{0.7}Co_{0.3}$ particles from 9.7 to 14.3 nm yields an increase of K_{eff} by a factor of about 4, while the bulk value is reached again for the smaller particles.[23] More experimental work is needed to elucidate this effect in detail.

Another parameter that can be obtained from $M(T)$ curves is the irreversibility temperature T_{irr} (the temperature at which M_{ZFC} and M_{FC} finally coincide). It is related to the blocking of the biggest particles. For an ideal superparamagnetic material, T_B and T_{irr} are identical so that their difference provides a good indicator of the actual particle size distribution.[24] For our samples, $M_{ZFC}(T)$ and $M_{FC}(T)$ clearly show irreversibility persisting up to T_{irr} higher than T_B.

Magnetization as a Function of Magnetic Field. The magnetic field dependences of the magnetization $M(H, T)$ at different temperatures have been measured for the FeCo@C and FeNi@C samples. From typical results of the $M(H, T)$ curves in expanded views shown in the insets of Figure 3, one observes that the coercivity possesses nonzero values from 5 K to certain temperature values (180 and 50 K for FeCo@C and FeNi@C samples, respectively) deducing blocking of the nanoparticles below these temperatures. The similarity of the hysteresis loops confirms the good stability of the synthesized

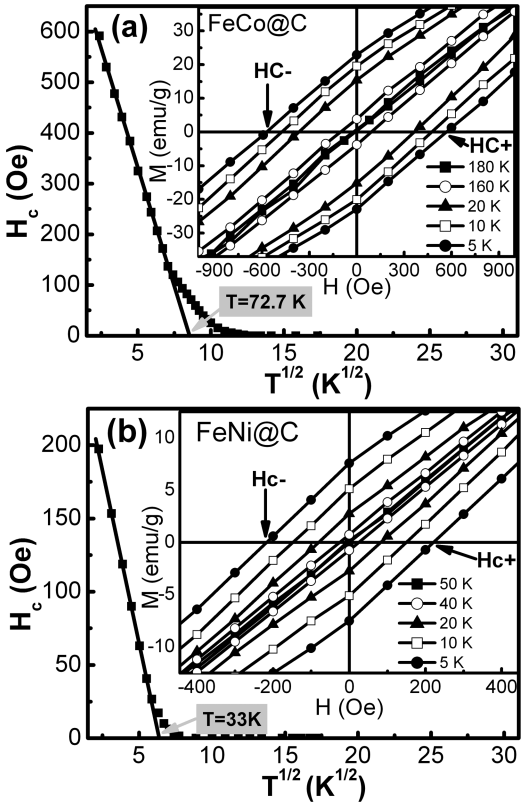

Figure 3. Temperature dependence of the coercivity (H_C) for (a) FeCo@C and (b) FeNi@C nanocomposites. The lines correspond to a linear fit based on eq 2. The insets show the corresponding low magnetic field region of the $M(H, T)$ curves measured at different temperatures.

dx.doi.org/10.1021/jp304236x | J. Phys. Chem. C 2012, 116, 22509−22517

Table 1. Physical Properties of the Magnetic Nanocomposites[a]

sample	d_{XRD} (nm)	d_{TEM} (nm)	$d_{coercivity}$ (nm)	H_{C0} (Oe)	d_{SL} (nm)	$d_{log\text{-}normal}$ (nm)	T^* (K)
FeCo@C	6.4 ± 1	5.9 ± 1	5	644 ± 5	4	4.6	925
FeNi@C	5.3 ± 1	4.6 ± 0.3	4.4	350 ± 5	4.2	4.5	263

[a]The average diameter values d_{XRD}, d_{TEM}, $d_{coercivity}$, d_{SL}, $d_{log\text{-}normal}$, determined from x-ray diffractogram, HRTEM images, H_c vs $T^{1/2}$ curve, simple Langevin function and log-normal weighted Langevin function, respectively; the experimentally extrapolated H_{C0} values and the room temperature values of the parameter T^* appears in the denominator of eq 6.

samples against oxidation. As known, the particles of these alloys could be covered by a thin oxide surface shell when exposed to air at room temperature unless protected by some other layer of stable material.[25,26] If oxide shells were present and the nanoparticles were cooled under a magnetic field, a significant difference in the magnitudes of the coercivity fields measured at the positive (H_{C+}) and negative (H_{C-}) sides of the magnetic field axes would arise (appear as shifts for the hysteresis loops toward negative fields) due to the exchange bias.[27,28] We have found that the values of (H_{C+}) and (H_{C-}) are equal within the uncertainty limits of the procedure employed to determine H_c (~2 Oe). This constitutes additional evidence for the absence of oxides surface shells around the nanoparticles and represents high stability against oxidation. It is worth noting that the magnetic measurements were repeated after 3 months and the results were the same.

Extracting the coercivity field H_c at different temperatures enables us to build the H_C versus $T^{1/2}$ diagram (as shown in Figure 3). For systems consisting randomly oriented and noninteracting superparamagnets, the behavior is described by the relation[18]

$$H_C = H_{C0}\left[1 - \frac{T}{T_B}\right]^{1/2} \quad (2)$$

where T_B is the blocking temperature and H_{C0} is the zero temperature coercivity. It is apparent from the figure that the behavior for both samples is a thermally activated process and H_C decreases linearly with $T^{1/2}$, mainly at temperatures below 73 and 33 K for FeCo@C and FeNi@C samples, respectively. By substituting these blocking temperature values in eq 1, we have found that the average diameters $d_{coercivity}$ are equal to 5 and 4.4 nm for FeCo@C and FeNi@C samples, respectively. The extrapolated values of H_{C0} for both samples are tabulated in Table 1. However, the zero temperature coercivity can be calculated using the expression $H_C(0) = 0.64K_{eff}/M_s$, which is assumed to be appropriate for the randomly oriented and noninteracting magnetic particles.[29] A significant difference can be expected between the calculated $H_C(0)$ and the experimentally extrapolated H_{C0} values and can be attributed to different mechanisms, including an incoherent magnetization reversal processes related to weak interactions such as fanning and curling, which are expected to decrease the zero temperature coercivity.[30] These processes are frequently observed in nanometric scale systems and believed to reduce the reversing field down to ~30% of the value calculated for rotation in unison (i.e., in the case of all spins remain parallel to each other throughout the reversal process).[31] In fact, for our samples the difference is much higher than this ratio, suggesting an appreciable contribution from the dipolar interaction resulted from the high concentration of the magnetic materials incorporated in the carbon matrix. The dipolar interactions induce an evolution of the magnetization reversal toward more incoherent and heterogeneous mechanisms, thus, reducing the zero temperature coercivity appreciably. Additionally, the contribution of shape anisotropy of individual nanoparticles cannot be neglected where the deviation from spherical shape of FeCo and FeNi nanoparticles are deduced by HRTEM investigation.

Several $M(H)$ curves were taken also at $T_B < T < 300$ K for the nanocomposites to study the magnetic field dependence of the magnetization at the high temperature range. At room temperature, the saturation magnetization M_s amounts to 112 and 48 emu/g for FeCo@C and FeNi@C nanocomposites, respectively. While for alloys a detailed experimental study is missing, for small Fe, Ni, and Co clusters, the magnetization is enhanced as compared to the bulk values M_S^{bulk} for clusters with less than 500−350 atoms.[32] For larger clusters, the saturation magnetization is in agreement with M_S^{bulk}.[33] The nanoparticles at hand consist of a more than one magnitude larger number of atoms so that we assume the relative saturation magnetization $M_S^{FeM@C}/M_S^{bulk}$ being a reliable measure of the actual magnetic mass fraction in our FeM@C composites. This assumption is corroborated by a recent study of Desvaux et al. in which magnetization values of FeCo nanoparticles close to those expected for the bulk alloy are reported if structural disorder is removed by annealing.[34] By neglecting the small diamagnetic response of the carbon matrix, the data yield mass ratios of about 45 and 28% of the total samples mass for FeCo@C and FeNi@C nanocomposites, respectively.

The $M \times H$ cycles are characterized by (a) nonhysteretic behavior where the coercivity remains zero and (b) scaling onto a universal curve of normalized M/M_S versus H/T, as has been illustrated in Figure 4. In addition, Figure 4 shows the fitting results of magnetization isotherms ($M-H$ curves) measured at different temperatures for both samples assuming both simple and log-normal weighted Langevin functions. The utilization of simple Langevin function results in poorer fit of the experimental data with estimated diameter values d_{SL} similar with d_{TEM} for FeNi@C nanocomposite but relatively lower in the case of FeCo@C nanocomposite (see Table 1).

Based on the HRTEM results, the magnetization of our superparamagnetic nanoparticles is expected to be better represented by considering a weighted sum of Langevin functions that takes into account a distribution of magnetic moment due to the particle size distribution.[31,35] The optimal fitting achieved to the log-normal weighted Langevin function by considering medians of the distribution $\mu_0 = 6.03 \times 10^{-17}$ and 3.8×10^{-17} emu for FeCo@C and FeNi@C samples, respectively. The mean diameters $d_{log\text{-}normal}$ calculated from these values are 4.6 and 4.5 nm for FeCo@C and FeNi@C samples, respectively, which agrees well with the results of the TEM and XRD analysis.

From the magnetic properties discussed above, one can observe that the FeNi@C nanocomposite can be described as superparamagnetic on the basis of the following points: (a) the nonhysteretic $M(H)$ curves are well described in terms of

dx.doi.org/10.1021/jp304236x | J. Phys. Chem. C 2012, 116, 22509−22517

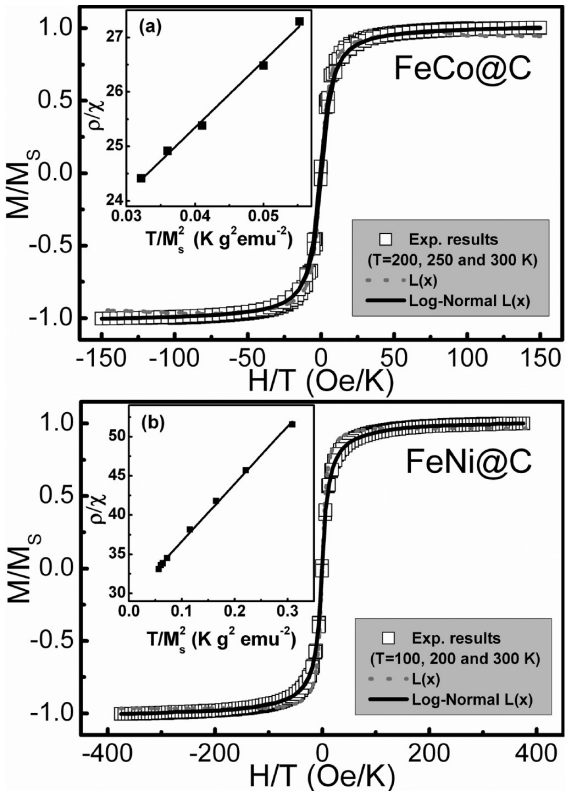

Figure 4. Normalized magnetization as a function of H/T at different temperatures for the magnetic nanocomposite. Fitting based on the simple and the log-normal weighted Langevin functions are illustrated. The insets clarify the linear relation of ρ/χ vs TM_S^2 plots; for details, see text.

Langevin functions; (b) the H/T scaling with the normalized magnetization; (c) the blocking process appears at nearly unique temperature and followed with paramagnetic-like behavior. However, the behavior of the FeCo@C nanocomposite is puzzling. For this nanocomposite, the deviations appearing from the simple superparamagnetic behavior due to existence of strong interactions between the nanomagnets can be a criticizing point for describing it as a superparamagnetic system. However, it is reasonable to assume that it is not sufficiently strong to overwhelm the superparamagnetic features of the FeCo@C nanocomposite if the first two points discussed above are taken in consideration. The best description is that the nanocomposite is an interacting superparamagnetic (ISP) system. As has been reported for magnetic nanocomposites with similar behavior,[9] the magnetization of interacting moments can also be represented by the Langevin function, which is appropriate for noninteracting moment; but in such a case the estimated magnetic moment and, hence, the particle size are lower than the real one.[36] In conclusion, the fit of nonhysteretic behavior of the $M(H)$ curves with Langevin function does not contradict with the presence of the dipolar interactions, which is reasonable in the composites of high volume fraction of magnetic nanoparticles[1,31,37] like we have studied in this work.

Dipolar Interaction between the Nanoparticles. Some applications of the magnetic nanocomposites especially in medical fields require the preparation of stable liquid suspensions of magnetic particles. As discussed above, the synthesized nanocomposites are superparamagnetic nanocrystals dispersed inside submicrometer-scaled spherical diamagnetic colloide. Because of this particular microstructure, the nanocomposites are expected to have long sedimentation times in the absence of a magnetic field.[8,26] For superparamagnetic solutions, the dipolar interactions have significant effect on the sedimentation time, a matter that gives interest to analyze the presence of the dipolar interactions between the magnetic nanoparticles in the nanocomposite under study. In this work a comprehensive analysis of the presence of dipolar interactions has been carried out within the framework of mean-field model proposed by Allia et al.[36] and verified by Binns et al.[9] The use of this model could allow estimating the dipolar interactions in a temperature region within which the interacting superparamagnetic regime (ISP) describes the behavior of interacting nanomagnets. According to this model, the dipolar interaction can be characterized by a parameter T^* appearing in the denominator of Langevin function analogous to the Curie–Weiss law, that is,

$$M = N\mu L\left(\frac{\mu H}{k_B(T + T^*)}\right) \tag{3}$$

where N is the number of moments per unit volume, L is the Langevin function, k_B is the Boltzmann constant, μ is the particle moment, H is the magnetic field, and T is the temperature. The parameter T^* is proportional to the dipolar energy and can be given by the following formula:[36]

$$T^* = \frac{\alpha}{k_B}\frac{M_S^2}{N} \tag{4}$$

where α is a proportionality constant derived from the sum of all dipolar energy contributions.[38] α and N can be obtained from the low-field susceptibility data χ using the expression

$$\frac{\rho}{\chi} = 3k_B N\left(\frac{T}{M_S^2}\right) + 3\alpha \tag{5}$$

where ρ is $\langle\mu^2\rangle/\langle\mu\rangle^2$ ($\langle\mu\rangle$ and $\langle\mu\rangle^2$ being the average values of the particle moment and of its square). The linear dependence of the quantity ρ/χ on the ratio T/M_S^2 displayed in insets of Figure 4 supports the picture of the interacting superparamagnetic regime for both nanocomposites.[8,37,39] The values of T^* determined from the best linear fits are tabulated in Table 1. The FeCo@C sample has a relatively high value, indicating the high dipolar interaction between the nanomagnets, while the small value of T^* for FeNi@C sample indicates weaker dipolar interaction. To understand these results, one can take into consideration that the dipolar interactions scale with $\mu^2 r^6/D^3$, where μ is the magnetic moment, r is the particle radius, and D is the distance between the magnetic nanoparticles.[1] So it seems reasonable for FeNi@C to have relatively low values of T^* as a result of the small size of its nanomagnets and the large separating distance between them,[40] as has been shown by HRTEM images (see Figure 2d,f), as well as the smaller value of the magnetic moment.

Heating in AC Magnetic Fields for Magnetic Hyperthermia. To investigate and to quantify the feasibility of the FeCo@C and FeNi@C nanocomposites for magnetic hyperthermia, the effect of applied AC magnetic fields has been studied. To be specific, the temperature versus time dependence $T(t)$ was studied upon application of AC magnetic fields with a fixed frequency of 120 kHz at various magnetic field strengths up to 80 kA/m. The experiments have been performed on suspensions of the nanocomposites in aqueous

dx.doi.org/10.1021/jp304236x | J. Phys. Chem. C 2012, 116, 22509–22517

solutions of human albumin (5 mg/mL). The concentration of the nanocomposite in the suspension was chosen to be 5 mg/mL, and human albumin was utilized as biocompatible surfactant. The particles were dispersed by means of a tip sonicator for 2 min.

The heating effect of external alternating magnetic field with a frequency of 120 kHz and amplitudes of 20−80 kA/m on the aqueous suspension of the FeCo@C and FeNi@C nanocomposites is presented in Figure 5. The data imply significant

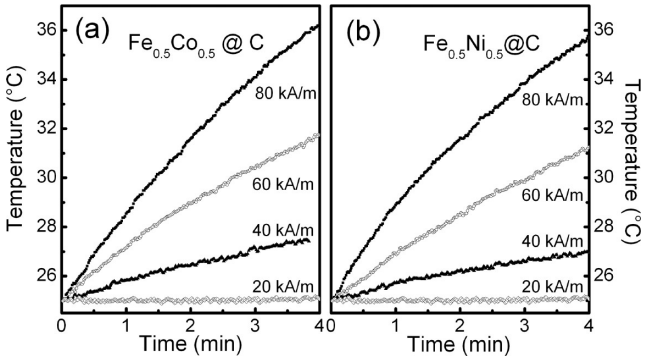

Figure 5. Temperature vs time of the FeCo@C and FeNi@C suspensions upon application of AC magnetic field with f = 120 kHz and different amplitudes between 20 and 80 kA/m, switched on at t = 0.

heating effects for field strengths ≥40 kA/m. A quantitative measure of the actual heating efficacy is the specific absorption rate SAR,[41]

$$\mathrm{SAR} = C\frac{\mathrm{d}T}{\mathrm{d}t}\frac{1}{m^*} \tag{6}$$

where C is the specific heat of water, $\mathrm{d}T/\mathrm{d}t$ is the initial slope of the temperature raise, and $m^* = m_{NP}/m_s$ is the mass of the active particle content m_{NP} divided by the total suspension mass. The results are shown in Figure 6, where for comparison SAR is plotted with respect to the total mass of the nanocomposites. For comparison with literature data on noncoated material, the data at 80 kA/m have been normalized

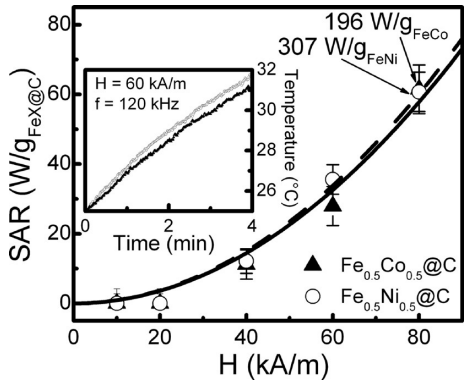

Figure 6. Specific absorption rate SAR of the FeCo@C and FeNi@C suspensions vs amplitude of the external AC magnetic field (f = 120 kHz). Data have been normalized to the total nanocomposite mass. For comparison, SAR(80 kA/m) normalized to the bare magnetic material is given, too. The lines display functions $\mathrm{SAR}(H) = a\cdot H^2$ with a fitting parameter a. Inset: Heating curves $T(t)$ for both materials at H = 60 kA/m.

to the active magnetic material only as extracted from the saturation magnetization. For both materials, there is a quadratic magnetic field amplitude dependence of the SAR, which is in agreement with the linear response theory (LRT) for superparamagnetic particles and confirms the magnetic origin of the heating effect.[42] Both materials exhibit very similar heating efficacy, as evidenced by the similar SAR values and the very similar temperature dependencies (see the inset of Figure 6). However, as the amount of active magnetic material FeCo (45 wt %) in FeCo@C is much higher than that of FeNi (28 wt %) in FeNi@C, as extracted from the magnetization data, this coincidence does not imply similar heating ability of the core particles in the two materials. A priori, we expect different heating ability of the FeCo and FeNi cores. In addition, the distribution in the C matrix is relevant, too, which is better for the FeNi nanoparticles (see Figure 1c,d). Improvement of the distribution results in a significantly better heating of the composite, that is, the specific absorption rate of nanomaterial increases due to a decrease in interparticle interactions.[2]

Generally, heat dissipation in magnetic nanoparticles is associated with a lag of the magnetization with respect to the applied external field giving rise to a finite imaginary part of the susceptibility and, hence, energy conversion into heat if the relaxation time τ of the system is longer than the time of magnetic field reversal. In the case of nanoparticles, the underlying mechanism is either the Néel or the Brownian relaxation, or a mixture of both, and the associated relaxation times[43]

$$\tau_N = \tau_0 \exp\left(\frac{KV}{k_B T}\right), \quad \tau_B = \frac{3\eta V_h}{k_B T}, \quad \tau_{eff} = \frac{\tau_N \cdot \tau_B}{\tau_N + \tau_B} \tag{7}$$

with the Nèel, Brownian, and effective relaxation times τ_N, τ_B, and τ_{eff}, respectively. τ_0 is the attempt frequency usually in the range 10^{-9}−10^{-11} s, K is the anisotropy constant, V is the volume, V_h is the hydrodynamic volume of the particle, η is the viscosity, and k_B is the Boltzmann constant.

The power loss P corresponding to relaxation is given by[44]

$$P = \pi\mu_0\chi_0 H^2 f \frac{2\pi f\tau}{1 + (2\pi f\tau)^2} \tag{8}$$

where μ_0 is the magnetic permeability, χ_0 is the (field dependent) equilibrium susceptibility, H is the amplitude of the external driving field, and τ is the respective relaxation time. Maximum power loss appears at $2\pi f_r\tau = 1$. The Néel relaxation time at room temperature can be estimated from the magnetic anisotropy constants, that is, 3.8×10^5 and 2.5×10^5 J m^{3-} for FeCo@C (d = 5.9 ± 1 nm) and FeNi@C (d = 4.6 ± 1 nm) samples, respectively, by applying eq 7. By assuming $\tau_0 = 10^{-9}$ s, the data yield $\tau \sim 3 \times 10^{-5}$ s and f_r = 5.3 kHz (FeCo@C) and $\tau \sim 5 \times 10^{-5}$ s and f_r = 3.1 kHz (FeNi@C). Conversely, at our measurement frequency f = 120 kHz, the maximum Néel-type energy conversion appears for particles with $d \sim 5.3$ and 6.1 nm for FeCo@C and FeNi@C nanocomposites, respectively. We hence expect pronounced Néel-type dissipation effects in our materials, in particular, when considering the finite size distribution. In the materials at hand, the individual nanoparticles are embedded in large entities of carbon spheres. According to the TEM images (see Figure 1b), the average physical diameters of the spheres amount to ∼100 nm, which provides a lower boundary of the hydrodynamic size. Applying $\eta = 1 \times 10^{-3}$ Pa·s for water yields $\tau_B \sim 4 \times 10^{-4}$ s, that is, the

dx.doi.org/10.1021/jp304236x | J. Phys. Chem. C 2012, 116, 22509−22517

lower boundary for the dissipation maximum given by $2\pi f\tau = 1$ is about $f \sim 0.4$ kHz. A Brown-type relaxation can, hence, not be excluded at our measurement frequency of 120 kHz.

To compare the results quantitatively with other data, one may apply the SAR for calculating the intrinsic loss power (ILP), that is, SAR/(H^2f).[45] We find $ILP_{FeCo/FeNi@C} \sim 8 \times 10^{-5}$ nH $m^2/g_{FeCo/FeNi@C}$, $ILP_{FeCo} \sim 25 \times 10^{-4}$ nH m^2/g_{FeCo}, and $ILP_{FeNi} \sim 41 \times 10^{-4}$ nH m^2/g_{FeNi}. For comparison, a recent study on Co@C with 57 w% Co in the Co@C nanocomposite and mean core size of 9 nm yields $ILP_{Co@C} \sim 3 \times 10^{-4}$ nH $m^2/g_{Co@C}$ ($ILP_{Co} \sim 5.3 \times 10^{-4}$ nH m^2/g_{Co}).[46] Lacroix et al. studied pure (not coated) FeCo nanoparticles. Interestingly, the observed loss powers of our core materials clearly exceed the value ILS = 8.8×10^{-5} nH m^2/g_{FeCo} obtained on the pure $Fe_{0.63}Co_{0.37}$ nanoparticles.[47] Note, however, that it is not straightforward to compare the heating efficacy for a material because the particle size has an enormous effect, which is evident from the discussion of the relaxation time above. Experimentally, this is demonstrated, for example, in ref 45, where the ILP of various commercial iron oxide nanoparticles has been studied. Kallumadil et al. report that the highest ILP values of the studied samples of $\sim 3.1 \times 10^{-3}$ nH m^2/kg are achieved for particles with crystallite diameters of 12 nm, while it is about 1 order of magnitude lower for 8 nm in diameter particles. One, hence, can attribute the larger ILS values in our study to the fact that the size of the particles is nearer to the optimal size where Néel losses are maximal.

CONCLUSIONS

In this work, submicrometer-sized spheres of carbon colloid (with an average diameter 100 nm) containing randomly dispersed FeCo and FeNi nanoparticles (with average diameters 5.9 ± 1 and 4.6 ± 0.3 nm, respectively) are synthesized using a facile route. No indications of metal oxide phases were detected, suggesting that the synthesis method guarantees well carbon coating for the magnetic nanoparticles. The carbon shells could also be used for attaching therapeutic biomolecules, such as anticancer drugs, antibodies, and siRNA, to target tumor cells and tissues. The magnetization measurements confirm the superparamagnetic properties of the nanocomposites. Although the existence of dipolar interactions in the nanocomposites is confirmed, which was found to be higher for FeCo@C nanocomposite due to direct contacts between few neighbor FeCo nanoparticles, it was observed to be relatively low and does not lead to magnetic agglomeration between the spheres. These particular features of the spheres make them easy to disperse in different solutions typically used for biomedical applications. The heating response of the magnetic nanospheres in the AC magnetic field was tested where both nanocomposites exhibit substantial temperature increase in the liquid dispersion. The results obviously prove the feasibility of the use of the nanocomposites as hyperthermia agents.

AUTHOR INFORMATION

Corresponding Author

*Tel.: (+49) 351 4659315. Fax: (+49) 351 4659313. E-mail: e.ibrahim@science.sohag.edu.eg.

Notes

The authors declare no competing financial interest.

ACKNOWLEDGMENTS

The authors are grateful to Sieglinde Pichl and Gesine Kreutzer for help with SEM and HRTEM measurements. Authors would like to express their gratitude to Dietmar Meiler and Alexander Schubert for the technical support during the experimental work. Financial support by the Deutsche Forschungsgemeinschaft DFG under Contracts HA 5133/4-1 and WO 1532/1-2 is gratefully acknowledged.

REFERENCES

(1) Rebolledo, A. F.; Fuertes, A. B.; Gonzalez-Carreño, T.; Sevilla, M.; Valdes-Solis, T.; Tartaj, P. *Small* **2008**, *4*, 254−261.
(2) Rovers, S. A.; Dietz, v; Poel, L. A.; Hoogenboom, R.; Kemmere, M. F.; Keurentjes, J. T. *J. Phys. Chem. C* **2010**, *114*, 8144−8149.
(3) Klingeler, R.; Hampel, S.; Büchner, B. *Int. J. Hyperthermia* **2008**, *24*, 496−505.
(4) Poudyal, N.; Rong, V.; Liu, J. P. *J. Appl. Phys.* **2011**, *109*, 07B526.
(5) Chaubey, G. S.; Barcena, C.; Poudyal, V.; Rong, C.; Gao, J.; Sun, S.; Liu, J. P. *J. Am. Chem. Soc.* **2007**, *129*, 7214−7215.
(6) Hütten, A.; Sudfeld, D.; Ennen, I.; Reiss, G.; Hachmann, W.; Heinzmann, U.; Wojczykowski, K.; Jutzi, P.; Saikaly, W.; Thomas, G. *J. Biotechnol.* **2004**, *112*, 47−63.
(7) Hong, W.; Bai, H.; Xu, Y.; Yao, Z.; Gu, Z.; Shi, G. *J. Phys. Chem. C* **2010**, *114*, 1822−1826.
(8) Tartaj, P.; González-Carreño, T.; Bomatì-Miguel, O.; Serna, C. J. *Phys. Rev. B* **2004**, *69*, 094401.
(9) Gittleman, J. I.; Abeles, B.; Bozowski, S. *Phys. Rev. B* **1974**, *9*, 3891−3897.
(10) Cannas, C.; Musinu, A.; Piccaluga, G.; Fiorani, D.; Peddis, D.; Rasmussen, H. K.; Mørup, S. *J. Chem. Phys.* **2006**, *125*, 164714.
(11) Binns, C.; Maher, M. J. *Phys. Rev. B* **2002**, *66*, 184413.
(12) Batlle, X.; Labarta, A. *J. Phys. D: Appl. Phys.* **2002**, *35*, R15.
(13) Fernández-García, M. P.; Gorria, P.; Blanco, J. A.; Fuertes, A. B.; Sevilla, M.; Boada, R.; Chaboy, J. *Phys. Rev. B* **2010**, *81*, 094418.
(14) Martínez, B.; Obradors, X.; Balcells, L.; Rouanet, A.; Monty, C. *Phys. Rev. Lett.* **1998**, 181−184.
(15) Krupskaya, Y.; Mahn, C.; Parameswaran, A.; Taylor, A.; Krämer, K.; Hampel, S.; Leonhardt, A.; Ritschel, M.; Büchner, B.; Klingeler, R. *J. Magn. Magn. Mater.* **2009**, *321*, 4067−4071.
(16) Huang, Y.; Lin, J.; Bando, Y.; Tang, C.; Zhi, C.; Shi, Y.; Takayama-Muromachi, E.; Golberg, D. *J. Mater. Chem.* **2010**, *20*, 1007−1011.
(17) He, W. D.; Somarajan, S.; Koktysh, D. S.; Dickerson, J. H. *Nanoscale* **2011**, *3*, 184.
(18) Stoner, E. C.; Wohlfarth, E. P. *Philos. Trans. R. Soc., A* **1948**, *240*, 599−642.
(19) Bansmann, J.; Kleibert, A.; Getzlaff, M.; Rodríguez, A. F.; Nolting, F.; Boeglin, C.; Meiwes-Broer, K. *Phys. Status Solidi B* **2010**, *247*, 1152−1160.
(20) Margeat, O.; Ciuculescu, D.; Lecante, P.; Respaud, M.; Amiens, C.; Chaudret, B. *Small* **2007**, *3*, 451−458.
(21) Ammar, S.; Helfen, A.; Jouini, N.; Fievet, F.; Rosenman, I.; Villain, F.; Molinie, P.; Danot, M. *J. Mater. Chem.* **2001**, *11*, 186−192.
(22) El-Gendy, A. A.; Khavrus, V. O.; Hampel, S.; Leonhardt, A.; Büchner, B.; Klingeler, R. *J. Phys. Chem. C* **2010**, *114*, 10745.
(23) Peng, D. L.; Chena, Y.; Shea, H.; Katoh, R.; Sumiyama, K. *J. Alloys Compd.* **2009**, *469*, 276−281.
(24) Peddis, D.; Cannas, C.; Piccaluga, G.; Agostinelli, E.; Fiorani, D. *Nanotechnology* **2010**, *125705*, 1−10.
(25) Peddis, D.; Cannas, C.; Musinu, A.; Piccaluga, G. *J. Phys. Chem. C* **2008**, *112*, 5141−5147.
(26) Ibrahim, E. M. M.; Hampel, S.; Thomas, J.; Haase, D.; Wolter, A. U. B.; Khavrus, V. O.; Täschner, C.; Leonhardt, A.; Büchner, B. *J. Nanopart. Res.* **2012**, *14*, 1118.
(27) Fraune, M.; Rudiger, U.; Guntherodt, G.; Cardoso, S.; Freitas, P. *Appl. Phys. Lett.* **2000**, *77*, 3815−3817.
(28) Yao, Y. D.; Chen, Y. Y.; Tai, M. F.; Wang, D. H.; Lin, H. M. *Mater. Sci. Eng., A* **1996**, *217*, 281−285.

(29) Bozorth, R. M. *Ferromagnetism*; Van Nostrand, Princeton, N.J., 1956, Chap. 18, p 831.
(30) Cullity, J. B. D. *Introduction to Magnet*; Addison-Wesley: Reading, MA, 1972, Chap. 11.
(31) Fonseca, F. C.; Ferlauto, A. S.; Alvarez, F.; Goya, G. F.; Jardim, R. F. *J. Appl. Phys.* **2005**, *97*, 044313.
(32) Billas, I. M. L.; Chatelain, A.; de Heer, W. A. *Science* **1994**, *265*, 1682−1684.
(33) Khavrus, V. O.; Ibrahim, E. M. M.; Bachmatiuk, A.; Rümmeli, M.; Wolter, A. U. B.; Hampel, S.; Leonhardt, A. *J. Nanopart. Res.* **2012**, *14*, 914.
(34) Desvaux, C.; Amiens, C.; Fejes, P.; Renaud, P.; Respaud, M.; Lecante, P.; Snoeck, E.; Chaudret, B. *Nat. Mater.* **2005**, *4*, 750−753.
(35) Ferrari, E. F.; da Silva, F. C. S.; Knobel, M. *Phys. Rev. B* **1997**, *56*, 6086−6093.
(36) Allia, P.; Coisson, M.; Tiberto, P.; Vinai, F.; Knobel, M.; Novak, M. A.; Nunes, W. C. *Phys. Rev. B* **2001**, *64*, 144420.
(37) Tartaj, P.; Gonzalez-Carreño, T.; Serna, C. J. *Adv. Mater.* **2004**, *16*, 529−533.
(38) Kittel, C. *Introduction to Solid State Physics*; Wiley: New York, 1968.
(39) El-Gendy, A. A.; Ibrahim, E. M. M.; Khavrus, V. O.; Krupskaya, Y.; Hampel, S.; Leonhardt, A.; Büchner, B.; Klingeler, R. *Carbon* **2009**, *47*, 2821−2828.
(40) Bae, C.; Angappane, S.; Park, J. G.; Lee, Y.; Lee, J.; An, K.; Hyeon, T. *Appl. Phys. Lett.* **2007**, *91*, 102502.
(41) Andrä, W.; Nowak, H. *Magnetism in Medicine, A Handbook*, 2nd ed; Wiley-VCH: New York, 2007.
(42) Liu, C.; Zou, B.; Rondinone, A. J.; Zhang, Z. J. *J. Am. Chem. Soc.* **2000**, *122*, 6263−6267.
(43) Pankhurst, Q. A.; Connolly, J.; Jones, S. K.; Dobson, J. *J. Phys. D: Appl. Phys.* **2003**, *36*, R167−R181.
(44) Rosensweig, R. E. *J. Magn. Magn. Mater.* **2002**, *252*, 370−374.
(45) Kallumadil, M.; Tada, M.; Nakagawa, T.; Abe, M.; Southern, P.; Pankhurst, Q. A. *J. Magn. Magn. Mater.* **2009**, *321*, 1509−13.
(46) Lukanov, P.; Anuganti, V. K.; Krupskaya, Y.; Galibert, A.; Soula, B.; Tilmaciu, C.; Velders, A. H.; Klingeler, R.; Büchner, B.; Flahaut, E. *Adv. Funct. Mater.* **2011**, *21*, 3583−3588.
(47) Lacroix, L. M.; Malaki, R. B.; Carrey, J.; Lachaize, S.; Respaud, M.; Goya, G. F.; Chaudret, B. *J. Appl. Phys.* **2009**, *105*, 023911.